

Stabilized Ultra-High-Temperature Sensors Based on Inert Gas-Sealed Sapphire Fiber Bragg Gratings

Jia He, Xizhen Xu, Bin Du, Baijie Xu, Runxiao Chen, Ying Wang, Changrui Liao, Jinchuan Guo, Yiping Wang, and Jun He*

Cite This: *ACS Appl. Mater. Interfaces* 2022, 14, 12359–12366

Read Online

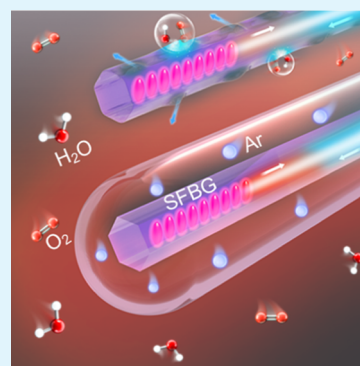
ACCESS |

Metrics & More

Article Recommendations

ABSTRACT: *In situ* measurement of high temperature is critical in aerospace, petrochemical, metallurgical, and power industries. The single-crystal sapphire fiber is a promising material for high-temperature measurement owing to its high melting point of ~ 2045 °C. Sapphire fiber Bragg gratings (SFBGs), which could be inscribed in sapphire fibers with a femtosecond laser, are widely used as high-temperature sensors. However, conventional SFBGs typically exhibit a significant deterioration in their spectra after long-term operation at ultra-high temperatures, resulting from the formation of some unwanted microstructural features, that is, lossy spots and micro-etched lines, on the surface of the sapphire fiber. Here, we report for the first time, to the best of our knowledge, a thermally stabilized ultra-high-temperature sensor based on an SFBG created by femtosecond laser inscription, inert gas-sealed packaging, and gradient temperature-elevated annealing. The results indicate that the lossy spots are essentially aluminum hydroxide induced by high-temperature oxidation, and the inert gas-sealed packaging process can effectively insulate the sapphire fiber from the ambient air. Moreover, the formation of micro-etched lines was suppressed successfully by using the gradient temperature-elevated annealing process. As a result, the surface topography of the SFBG after operating at high temperatures was improved obviously. The long-term thermal stability of such an SFBG was greatly enhanced, showing a stable operation at 1600 °C for up to 20 h. In addition, it could withstand an even higher temperature of 1800 °C with a sensitivity of 41.2 pm/°C. The aforementioned results make it promising for high-temperature sensing in chemical, aviation, smelting, and power industries.

KEYWORDS: optical fiber sensor, sapphire optical fiber, fiber Bragg grating, high temperature, inert gas-sealed packaging



1. INTRODUCTION

Temperature is one of the most common indicators used for condition monitoring in aviation, smelting, and power industries.^{1–4} There is a growing demand for ultra-high-temperature sensors to ensure safety and estimate performance deterioration. For example, the heart of an aircraft, the operating environment of the aeroengine, is extremely harsh, with the temperature inside its combustion chamber and turbine being up to ~ 1500 °C or even 1800 °C.^{1,5} Temperature monitoring in an aeroengine will be beneficial to extending its service life, obtaining higher combustion efficiency, and improving combustion mode in terms of reducing NO_x emissions.^{6,7} Commercial high-temperature sensors,^{8–15} such as thermocouples,¹⁶ temperature-sensitive paint,¹⁷ and infrared thermal imagers,^{18,19} have their own shortcomings. For example, thermocouples are susceptible to electromagnetic interference. In addition, they are single-point sensors, which are not conducive to distributed sensing. Temperature-sensitive paint and infrared thermal imagers can merely be suitable to measure the surface temperature.

Optical fiber-based devices, such as fiber Bragg gratings (FBGs), are more attractive for high-temperature sensing,

owing to their high sensitivity, compact size, capability of multiplexing, and immunity to electromagnetic interference. A femtosecond laser, featuring an ultra-short pulse width and an extremely high peak intensity, is a powerful tool for creating such functional devices (such as F-P interferometers,^{8,9} gratings,^{10–15} and microactuators²⁰) in or on almost all kinds of materials, for example, fibers without any photosensitivity (such as sapphire fibers) and metal.²¹ Various types of FBGs, including type I,^{10,11} type II,^{11–13} and regenerated FBGs,^{14,15} were studied and developed as high-temperature sensors. Compared with UV-induced type I FBGs, type II FBGs inscribed by using high-intensity femtosecond lasers can withstand temperatures above 1000 °C.^{10,22} However, the operating temperature of conventional silica-based FBGs is limited by the glass-transition temperature (~ 1330 °C).^{22,23}

Received: December 20, 2021

Accepted: February 8, 2022

Published: February 17, 2022



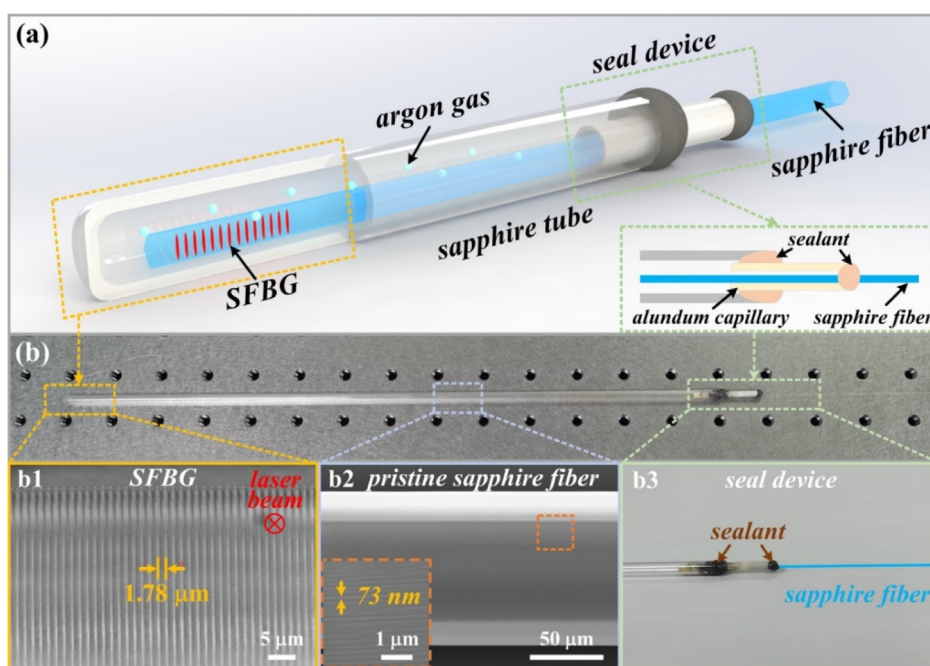


Figure 1. Ultra-high-temperature sensor based on an inert gas-sealed SFBG; (a) schematic of the sensor; (b) photograph of the sensor prototype. (Insets: b1, top-view microscopy image of the femtosecond laser-inscribed SFBG; b2, scanning electron microscopy image of the surface of the pristine sapphire fiber; b3, seal device of the sapphire tube.)

A single-crystal sapphire fiber, which has a high melting temperature of ~ 2045 °C, outstanding chemical resistance, and low transmission loss, is a promising candidate for fabricating ultra-high-temperature sensors. Blackbody radiation,²⁴ F-P interferometers,²⁵ Bragg grating,^{26–31} and Raman scattering³² on sapphire fibers have been reported for high-temperature sensing. In these methods, sapphire FBGs (SFBGs) exhibit a high mechanical strength, a high signal-to-noise ratio (SNR), and a capability for multiplexing. The highest short-term operating temperature of SFBGs reported so far was ~ 1900 °C.²⁷ As for the study on long-term stability, alumina tube-packaged SFBGs were reported to survive at a high temperature of 1000 °C for 110 h.³³ Moreover, in 1999, Shen *et al.* discovered the lossy spots formed on the surface of sapphire fibers after a high-temperature test, and those lossy spots could result in serious deterioration in the transmission performance of the sapphire fibers.^{35–37} Later, the researchers at Ohio State University found that the lossy spots were formed by high-temperature oxidation.^{36,37} Wilson *et al.* proposed an effective method to solve this problem by packaging the sapphire fiber *via* a pure alumina tube infiltrated with inert gas, and hence the attenuation of sapphire fibers at high temperatures can be reduced.³⁷ Nevertheless, to the best of our knowledge, there are few reports on the long-term stability of SFBGs at temperatures higher than 1600 °C, at which the degeneration of SFBGs will occur due to the absence of a protective cladding and the thermal reaction at the fiber–air interface.³⁴

In this paper, we discovered the micro-etched lines and lossy spots formed on the surface of sapphire fibers after long-term operation at ultra-high temperatures. We characterized the two microstructural features and found that the lossy spots are essentially some form of aluminum hydroxide formed by a chemical reaction between the sapphire fiber and air, and the micro-etched lines are caused by non-uniform residual stress relaxation. As shown in Figure 1, we propose a new method to

suppress the formation of such unwanted microstructural features on the surface of SFBGs by using an inert gas-sealed packaging and gradient temperature-elevated annealing process. Hence, the surface topography of the sapphire fiber can be improved, leading to the enhancement of long-term thermal stability of SFBGs. Such an SFBG can stably operate at 1600 °C for up to 20 h and withstand an ultra-high temperature of 1800 °C with a sensitivity of 41.2 pm/°C. The characteristics mentioned above make it promising for chemical, aviation, smelting, and power industries.

2. DEVICE FABRICATION

As shown in Figure 1, the proposed ultra-high-temperature sensor consists of an SFBG inscribed with a femtosecond laser line-by-line technique²⁹ and sealed in an argon gas-infiltrated sapphire tube by using a handmade seal device. The SFBG, as shown in the inset (b1) of Figure 1, was inscribed on the tip of a commercial single-crystal sapphire fiber (MicroMaterial, diameter: 100 μm , length: ~ 50 cm) by using appropriate fabrication parameters, including a single-pulse energy of 29.9 nJ, a track length of 60 μm , a grating pitch of 1.78 μm , and a grating length of 2 mm.

A commercial sapphire tube (Crytur, inner diameter: 3.4 mm) was selected for packaging the SFBG since it has a high melting temperature of ~ 2000 °C, similar to that of a single-crystal sapphire fiber. Such a sapphire tube also has excellent chemical corrosion resistance and great mechanical strength and hence could be used for protecting an SFBG from pollution and breakdown in high-temperature environments. Moreover, argon gas infiltrated into the sapphire tube could further protect the SFBG from high-temperature oxidation due to its chemical inertness.³⁷ Before argon infiltration, as shown in Figure 1, an alumina capillary (outer diameter: 2 mm, inner diameter: 1 mm) was inserted into the opening end of the sapphire tube and sealed using a high-temperature sealant (Shuoxian, SX-8301) *via* a hand-held dispensing process and

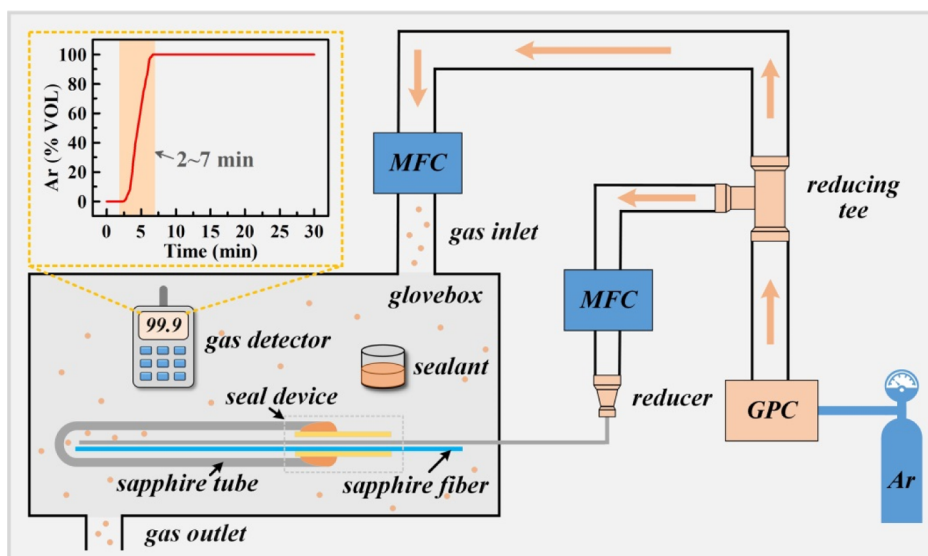


Figure 2. Experimental setup for sealing the fabricated SFBG in a sapphire tube with inert gas (MFC, mass flow controller; GPC, gas pressure controller). (Inset: the evolution of argon concentration inside the glovebox during the gas infiltrating process.)

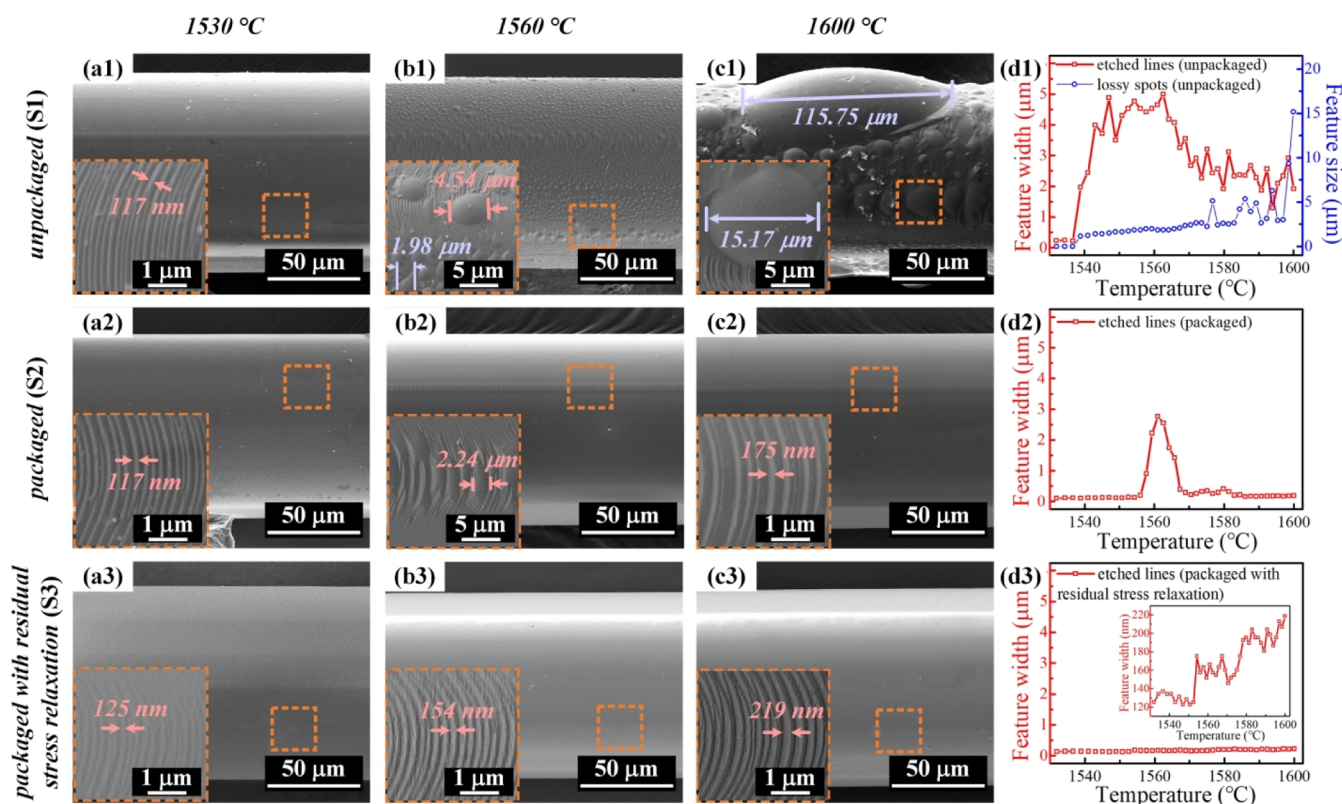


Figure 3. SEM images showing the surface topography of three sapphire fiber samples S1–S3 after long-time high-temperature annealing at (a1–a3) 1530 °C, (b1–b3) 1560 °C, and (c1–c3) 1600 °C. (d1–d3) Evolutions of the feature size of lossy spots and feature width of the etched lines on the surface of the fiber samples (S1, unpacked sample; S2, packaged sample; S3, packaged sample with stress relaxation).

cured at 70 °C for 2 h. Then, the fabricated SFBG was threaded into the sapphire tube through the alundum capillary and placed into a glovebox. The experimental setup for argon gas infiltration is shown in Figure 2. The argon gas flows into the sapphire tube with a precisely controlled flow rate *via* a gas pressure controller (General Electric, Druck PACE6000) and two mass flow controllers (Sevenstar, CS200A). During this period, the concentration of argon in the glovebox was real-time monitored by a high-precision gas detector (Kunlian,

KL400-Ar-Y). The argon concentration quickly increased to 99.9% after 7 min, and the filling process lasted for 30 min to ensure a full infiltration of argon. The opening end of the alundum capillary was then sealed, and an inert atmosphere could be maintained in the sealed sapphire tube. As a result, as shown in Figure 1b, an inert gas-sealed SFBG sensor prototype was obtained.

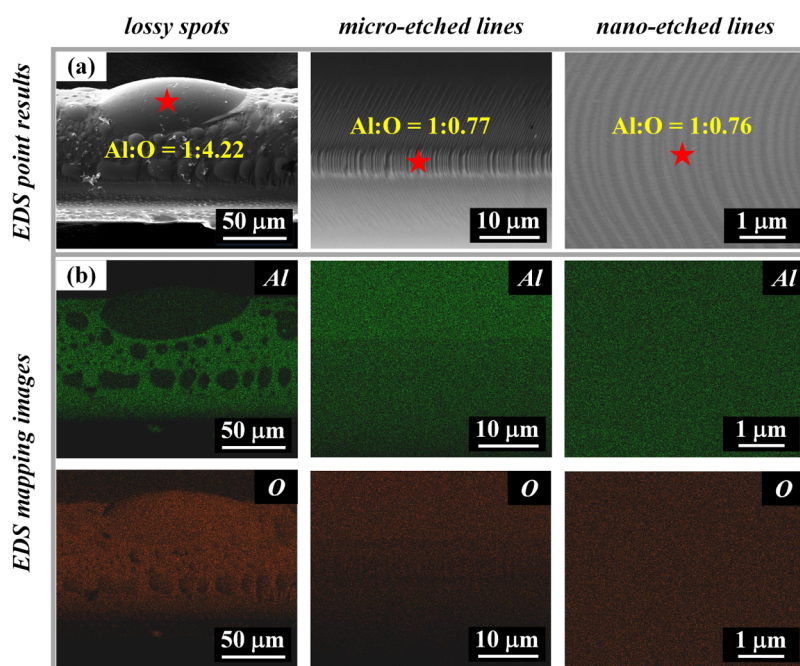


Figure 4. (a) EDS point results and (b) mapping images of the microstructural features, including lossy spots, micro-etched lines, and nano-etched lines, on the surface of the sapphire fiber.

3. RESULTS AND DISCUSSION

3.1. Characterization. The surface topography of sapphire fibers after high-temperature annealing was studied using a scanning electron microscope (TESCAN, LYRA3 XMH). At first, the SEM image of a pristine sapphire fiber was captured, showing a very smooth surface topography in the inset (b2) of Figure 1. Then, two sapphire fibers, one without packaging (S1) and the other one with inert gas-sealed packaging (S2), were isothermally annealed at 1600 °C for 55 h in a tube furnace (Carbolite, Gero HTRH). A B-type thermocouple was used to monitor the interior temperature of the furnace, which increased from room temperature to 1600 °C at a speed of 3 °C/min. After the high-temperature annealing process, the SEM images of two samples were taken. In the case of the unpackaged sample (S1), as shown in Figure 3a1–c1, some bubbles, so-called lossy spots, could be seen on the fiber surface, along the entire length of heated region. The feature size of lossy spot, as shown in the blue line in Figure 3d1, increases drastically at temperatures higher than 1590 °C. The feature size of lossy spots on the sapphire fiber at 1600 °C, which are marked by blue lines in Figure 3c1, is typically $\sim 15 \mu\text{m}$ and can reach a maximum of $115.75 \mu\text{m}$. The formation of lossy spots could be explained by a chemical reaction between the sapphire material and the surrounding atmosphere at high temperatures.³⁶ Moreover, another microstructural feature (*i.e.*, etched lines), with a feature width from sub-microns to several microns, is shown in Figure 3 and are marked by red lines. The micro-etched lines were unevenly formed in clusters or groups and occupied a certain area on the surface of the sapphire fiber. As shown in the red line in Figure 3d1, in the case of temperature increase, the feature width of the micro-etched lines first increases and then decreases, exhibiting a maximum of $\sim 5 \mu\text{m}$. In general, the smoothness on the surface of the sapphire fiber deteriorates significantly at high temperatures.

In the case of the packaged sample (S2), the lossy spots almost disappear, shown in Figure 3a2–c2, which means that

the inert gas-sealed packaging is effective to suppress the formation of lossy spots. However, the etched lines can still be observed in the insets of Figure 3a–c2. The feature width of the micro-etched lines on S2 exhibits a similar trend to that of S1. However, the micro-etched lines merely appear on the section of the sapphire fiber annealed at 1560 °C, and the largest feature width decreases to $\sim 3 \mu\text{m}$. It is reasonable to predict that the micro-etched lines are caused by the non-uniform residual stresses.³⁸

Then, we fabricated another sapphire fiber sample (S3) with inert gas-sealed packaging and gradient temperature-elevated annealing, which can release the residual stress uniformly. The sample S3 was also isothermally annealed at 1600 °C for 55 h but in a slower heating process, that is, 1 h at 300 °C, 3 h at 600 °C, 6 h at 900 °C, 12 h at 1200 °C, 24 h at 1500 °C, and 55 h at 1600 °C. As shown in Figure 3a3–c3, the micro-etched lines disappear completely, except for some nano-etched lines on the surface. The feature width shows an upward trend in Figure 3d3 with increasing temperature. Note that these nano-etched lines on the annealed sapphire fiber sample S3 have a maximum width of $\sim 200 \text{ nm}$, which is still larger than that on a pristine sapphire ($\sim 70 \text{ nm}$) shown in the inset (b2) of Figure 1.

Furthermore, we analyzed the elementary composition of lossy spots and etched lines using an energy-dispersive X-ray spectroscope (FEI, Scios02). The EDS point results at locations marked by asterisks in Figure 4a illustrate that the lossy spots have an Al/O ratio of 1:4.22, which is much lower than that of 1:0.79 in the pristine sapphire fiber. This means the lossy spots result from high-temperature oxidation, that is, they could be regarded as aluminum hydroxide.^{39,40} Moreover, the micro-etched lines and nano-etched lines have Al/O ratios of 1:0.77 and 1:0.76, respectively, which are similar to that of the pristine sapphire fiber. Then, as displayed in Figure 4b, the mapping images show that the lossy spots have decreased aluminum content obviously. In addition, these two types of etched lines have an aluminum content on the surface similar

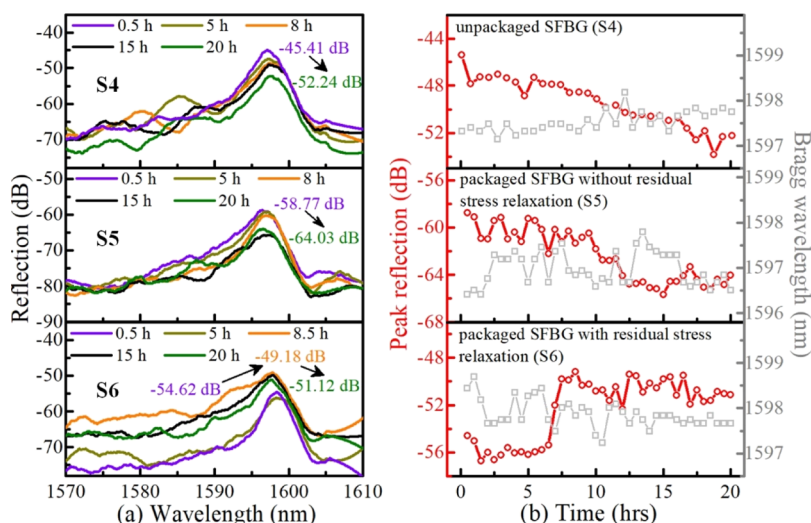


Figure 5. (a) Reflective spectral evolutions of three different SFBG sensors S4–S6 after 20 h of annealing at 1600 °C. (b) Evolutions of peak reflection and Bragg wavelength of S4–S6 with the annealing time at 1600 °C.

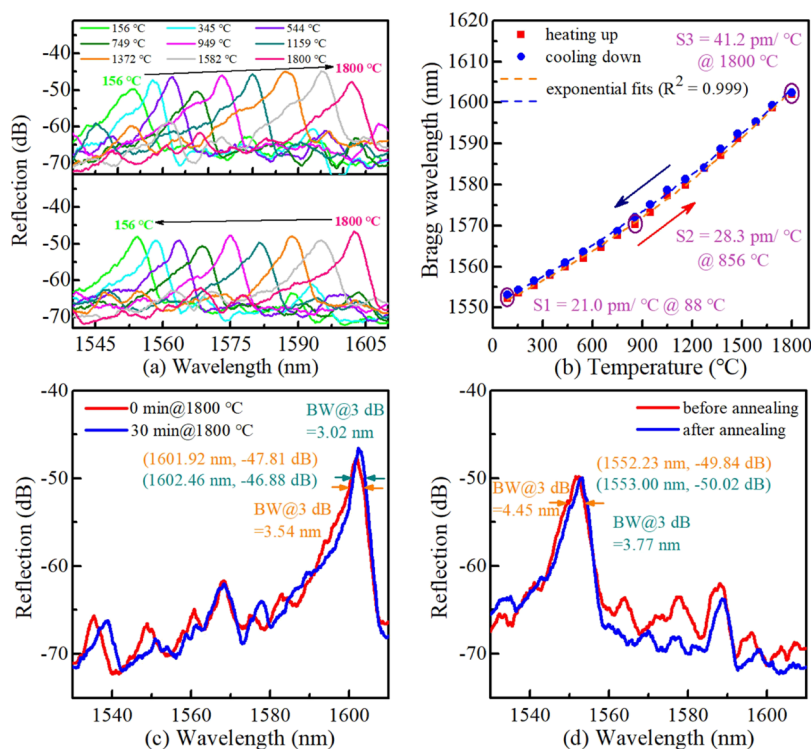


Figure 6. (a) Reflective spectral evolution of an inert gas-sealed SFBG with temperature in the heating and cooling process. (b) Bragg wavelength of the inert gas-sealed SFBG as a function of temperature cycling from 88 to 1800 °C. (c) Reflective spectra of an SFBG after 30 min of annealing at 1800 °C. (d) Reflection spectra of an SFBG at 88 °C before and after annealing.

to that of the pristine sapphire fiber. It means that the etched lines should not be introduced by a chemical reaction; instead, it might be introduced by a thermal volatilization process, in which the sapphire material can sublime into a vapor phase.^{38,40}

3.2. Temperature Measurement. Subsequently, we evaluated the long-term thermal stability of three fabricated high-temperature sensors, that is, a sample without packaging (S4), a sample with inert gas-sealed packaging (S5), and a sample with inert gas-sealed packaging and gradient temperature-elevated annealing (S6) by placing them in the center section of the tube furnace to ensure a stabilized high-

temperature condition. An optical frequency domain reflectometer (Luna, OBR 4600) was used to interrogate the SFBG sensor during the high-temperature test. One end of the sapphire fiber was connected to the lead-in multimode silica fiber (62.5/125 μm) by butt-coupling. To reduce the background reflection, the fiber connector was immersed in the index-matching oil. Three high-temperature sensors, that is, S4–S6, were isothermally annealed at 1600 °C for 20 h with different heating processes, that is, heating from room temperature to 1600 °C with a speed of 3 °C/min in the cases of S4 and S5 and gradient temperature-elevated annealing in the case of S6. Moreover, the reflection spectra

were recorded every 30 min, and Savitzky–Golay smoothing was applied on these reflection spectra to increase the accuracy in detecting the peak wavelength.

It can be seen from Figure 5a that three samples S4–S6 exhibit different SNR evolutions in their reflection spectra during the long-term high-temperature test. As shown in Figure 5b, the peak reflections of S4 and S5 after annealing at 1600 °C for 20 h decrease by ~ 7 and ~ 5 dB, respectively. This may result from the high-temperature-induced permanent defects on the fiber surface (*i.e.*, lossy spots and etched lines), which can increase the attenuation of the sapphire fiber. In addition, the peak reflection of S6 increases by ~ 4 dB and still remains stable after annealing at 1600 °C for 20 h. This may result from the improvement of the surface topography of the sapphire fiber by using inert gas-sealed packaging and gradient temperature-elevated annealing. Moreover, as shown in Figure 5b, the Bragg wavelengths of S4–S6 fluctuate sharply in the first 17 h and then stabilize in the last 3 h. This indicates that the femtosecond laser-induced residual stress could be released by high-temperature annealing, and hence, a thermally stabilized SFBG ultra-high-temperature sensor could be achieved.⁴¹

Furthermore, we studied the temperature response of an inert gas-sealed SFBG sensor at higher temperatures, that is, the temperature was varied from 88 to 1800 °C and was maintained for 20 min at each measurement point. The complete temperature response of the packaged SFBG is shown in Figure 6a,b. It is obvious the Bragg wavelength of the SFBG exhibits a “red” shift with increasing temperature and a “blue” shift with decreasing temperature. Note that the peak reflection and SNR in the reflection spectra of the inert gas-sealed SFBG sensor have no severe deterioration in the heating and cooling process. The temperature sensitivities of the inert gas-sealed SFBG at various temperatures, that is, 21.0 pm/°C at 88 °C, 28.3 pm/°C at 856 °C, and 41.2 pm/°C at 1800 °C, were evaluated by applying exponential fits to the measured data. These results are consistent with those in previous works.^{26–31} However, such an inert gas-sealed SFBG has much better repeatability than the previous “naked” SFBGs.^{29–31} Furthermore, as shown in Figure 6c, the reflection spectrum of the inert gas-sealed SFBG remains almost unchanged at 1800 °C for 30 min. Figure 6d shows that the reflection spectrum of the inert gas-sealed SFBG can return to its initial state after annealing at 1800 °C except for a Bragg wavelength shift of 770 pm. Consequently, the excellent high-temperature sensing performance of such an inert gas-sealed SFBG sensor makes it promising for various ultra-high-temperature measurements.

4. CONCLUSIONS

We have proposed and demonstrated a new method for improving the long-term thermal stability of SFBGs by using an inert gas-sealed packaging and gradient temperature-elevated annealing process. The surface topography and the elementary composition of sapphire fibers after suffering a high temperature were studied. The results indicate that the lossy spots, essentially some form of aluminum hydroxide, can be suppressed effectively by using the inert gas-sealed packaging process, and non-uniform residual stresses can lead to the formation of micro-etched lines, which could be eliminated by gradient temperature-elevated annealing. Hence, the sapphire fiber with an improved surface topography after high-temperature annealing has been obtained. An SFBG ultra-high-temperature sensor created by femtosecond laser

inscription, inert gas-sealed packaging, and gradient temperature-elevated annealing has been achieved. The long-term high-temperature annealing test shows that such an SFBG sensor can operate at 1800 °C with a sensitivity of 41.2 pm/°C and is quite stable at 1600 °C for more than 20 h. Therefore, such a stabilized ultra-high-temperature sensor based on an inert gas-sealed SFBG could be potentially applied in many applications, such as chemical, aviation, smelting, and power industries.

AUTHOR INFORMATION

Corresponding Author

Jun He – Key Laboratory of Optoelectronic Devices and Systems of Ministry of Education/Guangdong Province, College of Physics and Optoelectronic Engineering, Shenzhen University, Shenzhen 518060, China; Shenzhen Key Laboratory of Photonic Devices and Sensing Systems for Internet of Things, Guangdong and Hong Kong Joint Research Centre for Optical Fibre Sensors, Shenzhen University, Shenzhen 518060, China; orcid.org/0000-0002-9417-2019; Email: hejun07@szu.edu.cn

Authors

Jia He – Key Laboratory of Optoelectronic Devices and Systems of Ministry of Education/Guangdong Province, College of Physics and Optoelectronic Engineering, Shenzhen University, Shenzhen 518060, China; Shenzhen Key Laboratory of Photonic Devices and Sensing Systems for Internet of Things, Guangdong and Hong Kong Joint Research Centre for Optical Fibre Sensors, Shenzhen University, Shenzhen 518060, China

Xizhen Xu – Key Laboratory of Optoelectronic Devices and Systems of Ministry of Education/Guangdong Province, College of Physics and Optoelectronic Engineering, Shenzhen University, Shenzhen 518060, China; Shenzhen Key Laboratory of Photonic Devices and Sensing Systems for Internet of Things, Guangdong and Hong Kong Joint Research Centre for Optical Fibre Sensors, Shenzhen University, Shenzhen 518060, China

Bin Du – Key Laboratory of Optoelectronic Devices and Systems of Ministry of Education/Guangdong Province, College of Physics and Optoelectronic Engineering, Shenzhen University, Shenzhen 518060, China; Shenzhen Key Laboratory of Photonic Devices and Sensing Systems for Internet of Things, Guangdong and Hong Kong Joint Research Centre for Optical Fibre Sensors, Shenzhen University, Shenzhen 518060, China

Baijie Xu – Key Laboratory of Optoelectronic Devices and Systems of Ministry of Education/Guangdong Province, College of Physics and Optoelectronic Engineering, Shenzhen University, Shenzhen 518060, China; Shenzhen Key Laboratory of Photonic Devices and Sensing Systems for Internet of Things, Guangdong and Hong Kong Joint Research Centre for Optical Fibre Sensors, Shenzhen University, Shenzhen 518060, China

Runxiao Chen – Key Laboratory of Optoelectronic Devices and Systems of Ministry of Education/Guangdong Province, College of Physics and Optoelectronic Engineering, Shenzhen University, Shenzhen 518060, China; Shenzhen Key Laboratory of Photonic Devices and Sensing Systems for Internet of Things, Guangdong and Hong Kong Joint Research Centre for Optical Fibre Sensors, Shenzhen University, Shenzhen 518060, China

Ying Wang – Key Laboratory of Optoelectronic Devices and Systems of Ministry of Education/Guangdong Province, College of Physics and Optoelectronic Engineering, Shenzhen University, Shenzhen 518060, China; Shenzhen Key Laboratory of Photonic Devices and Sensing Systems for Internet of Things, Guangdong and Hong Kong Joint Research Centre for Optical Fibre Sensors, Shenzhen University, Shenzhen 518060, China; orcid.org/0000-0001-8020-3622

Changrui Liao – Key Laboratory of Optoelectronic Devices and Systems of Ministry of Education/Guangdong Province, College of Physics and Optoelectronic Engineering, Shenzhen University, Shenzhen 518060, China; Shenzhen Key Laboratory of Photonic Devices and Sensing Systems for Internet of Things, Guangdong and Hong Kong Joint Research Centre for Optical Fibre Sensors, Shenzhen University, Shenzhen 518060, China; orcid.org/0000-0003-3669-5054

Jinchuan Guo – Key Laboratory of Optoelectronic Devices and Systems of Ministry of Education/Guangdong Province, College of Physics and Optoelectronic Engineering, Shenzhen University, Shenzhen 518060, China

Yiping Wang – Key Laboratory of Optoelectronic Devices and Systems of Ministry of Education/Guangdong Province, College of Physics and Optoelectronic Engineering, Shenzhen University, Shenzhen 518060, China; Shenzhen Key Laboratory of Photonic Devices and Sensing Systems for Internet of Things, Guangdong and Hong Kong Joint Research Centre for Optical Fibre Sensors, Shenzhen University, Shenzhen 518060, China

Complete contact information is available at:
<https://pubs.acs.org/10.1021/acsami.1c24589>

Author Contributions

J.H., X.X., and J.H. jointly conceived the idea. J.H., X.X., J.H., and B.D. designed and fabricated the devices, built the experimental setup, and performed the experiments. J.H., X.X., J.H., B.D., B.X., and R.C. analyzed the data. Y.W., C.L., and Y.W. assisted with the theory. J.H., X.X., and J.H. wrote the manuscript with contributions from all co-authors. All authors have given approval to the final version of the manuscript.

Notes

The authors declare no competing financial interest.

ACKNOWLEDGMENTS

We are grateful for financial support from the National Natural Science Foundation of China (NSFC) (61875128, 62005170, U1913212); the Guangdong Science and Technology Department (2019TQ05X113, 2019A151511114, 2021A1515110320); and the Shenzhen Science and Technology Innovation Program (RCYX20200714114538160, JCYJ20180507182058432, JCYJ20200109114020865).

REFERENCES

- (1) Pollock, T. M. Alloy Design for Aircraft Engines. *Nat. Mater.* **2016**, *15*, 809–815.
- (2) Li, Y.; Chen, L.; Wang, L.; Ma, J. Monitoring the Safety Status of a Blast Furnace Hearth Using Cooling Stave Heat Flux. *AIP Adv.* **2020**, *10*, 025308.
- (3) Huang, J.; Albero Blanquer, L.; Bonefacino, J.; Logan, E. R.; Alves Dalla Corte, D.; Delacourt, C.; Gallant, B. M.; Boles, S. T.; Dahn, J. R.; Tam, H.-Y.; Tarascon, J.-M. Operando Decoding of Chemical and Thermal Events in Commercial Na(Li)-Ion Cells via Optical Sensors. *Nat. Energy* **2020**, *5*, 674–683.
- (4) Hashemian, H. M. On-Line Monitoring Applications in Nuclear Power Plants. *Prog. Nucl. Energy* **2011**, *53*, 167–181.
- (5) Aussavy, D.; Bolot, R.; Montavon, G.; Peyraud, F.; Szyndelman, G.; Gurt-Santanach, J.; Selezneff, S. YSZ-Polyester Abradable Coatings Manufactured by APS. *J. Therm. Spray Technol.* **2016**, *25*, 252–263.
- (6) Williamson, R. C.; Stanforth, C. M. Measurement of Jet Engine Combustion Temperature by the Use of Thermocouples and Gas Analysis. *SAE Technical Paper 690433*, 1969; Vol. 78, pp 1598–1616.
- (7) Skowron, A.; Lee, D. S.; De León, R. R.; Owen, B. Greater Fuel Efficiency is Potentially Preferable to Reducing NO_x Emissions for Aviation's Climate Impacts. *Nat. Commun.* **2021**, *12*, 564.
- (8) Wei, T.; Han, Y.; Tsai, H.-L.; Xiao, H. Miniaturized Fiber Inline Fabry-Perot Interferometer Fabricated with a Femtosecond Laser. *Opt. Lett.* **2008**, *33*, 536–538.
- (9) Liu, Y.; Qu, S.; Li, Y. Single Microchannel High-Temperature Fiber Sensor by Femtosecond Laser-Induced Water Breakdown. *Opt. Lett.* **2013**, *38*, 335–337.
- (10) Canning, J. Fibre Gratings and Devices for Sensors and Lasers. *Laser Photon. Rev.* **2008**, *2*, 275–289.
- (11) Smelser, C. W.; Mihailov, S. J.; Grobncic, D. Formation of Type I-IR and Type II-IR Gratings with an Ultrafast IR Laser and a Phase Mask. *Opt. Express* **2005**, *13*, 5377–5386.
- (12) Li, Y.; Yang, M.; Wang, D. N.; Lu, J.; Sun, T.; Grattan, K. T. Fiber Bragg Gratings with Enhanced Thermal Stability by Residual Stress Relaxation. *Opt. Express* **2009**, *17*, 19785–19790.
- (13) Warren-Smith, S. C.; Nguyen, L. V.; Lang, C.; Ebandorff-Heidepriem, H.; Monroe, T. M. Temperature Sensing up to 1300 °C Using Suspended-Core Microstructured Optical Fibers. *Opt. Express* **2016**, *24*, 3714–3719.
- (14) Bandyopadhyay, S.; Canning, J.; Stevenson, M.; Cook, K. Ultrahigh-Temperature Regenerated Gratings in Boron-Codoped Germanosilicate Optical Fiber Using 193 nm. *Opt. Lett.* **2008**, *33*, 1917–1919.
- (15) He, J.; Wang, Y.; Liao, C.; Wang, C.; Liu, S.; Yang, K.; Wang, Y.; Yuan, X.; Wang, G. P.; Zhang, W. Negative-Index Gratings Formed by Femtosecond Laser Overexposure and Thermal Regeneration. *Sci. Rep.* **2016**, *6*, 23379.
- (16) Lei, J.-F.; Will, H. A. Thin-Film Thermocouples and Strain-Gauge Technologies for Engine Applications. *Sens. Actuators, A* **1998**, *65*, 187–193.
- (17) Liu, T.; Sullivan, J. P. *Pressure and Temperature Sensitive Paints*; Springer Berlin Heidelberg, 2005.
- (18) Bagavathiappan, S.; Lahiri, B. B.; Saravanan, T.; Philip, J.; Jayakumar, T. Infrared Thermography for Condition Monitoring – a Review. *Infrared Phys. Technol.* **2013**, *60*, 35–55.
- (19) Ciampa, F.; Mahmoodi, P.; Pinto, F.; Meo, M. Recent Advances in Active Infrared Thermography for Non-Destructive Testing of Aerospace Components. *Sensors* **2018**, *18*, 609.
- (20) Li, R.; Jin, D.; Pan, D.; Ji, S.; Xin, C.; Liu, G.; Fan, S.; Wu, H.; Li, J.; Hu, Y.; Wu, D.; Zhang, L.; Chu, J. Stimuli-Responsive Actuator Fabricated by Dynamic Asymmetric Femtosecond Bessel Beam for In Situ Particle and Cell Manipulation. *ACS Nano* **2020**, *14*, 5233–5242.
- (21) Zhu, S.; Bian, Y.; Wu, T.; Chen, C.; Jiao, Y.; Jiang, Z.; Huang, Z.; Li, E.; Li, J.; Chu, J.; Hu, Y.; Wu, D.; Jiang, L. High Performance Bubble Manipulation on Ferrofluid-Infused Laser-Ablated Microstructured Surfaces. *Nano Lett.* **2020**, *20*, 5513–5521.
- (22) Liao, C. R.; Wang, D. N. Review of Femtosecond Laser Fabricated Fiber Bragg Gratings for High Temperature Sensing. *Photonic Sens.* **2013**, *3*, 97–101.
- (23) Liu, X.; Zhou, J.; Zhou, S.; Yue, Y.; Qiu, J. Transparent Glass-Ceramics Functionalized by Dispersed Crystals. *Prog. Mater. Sci.* **2018**, *97*, 38–96.
- (24) Dils, R. R. High-Temperature Optical Fiber Thermometer. *J. Appl. Phys.* **1983**, *54*, 1198–1201.

(25) Zhu, Y.; Huang, Z.; Shen, F.; Wang, A. Sapphire-Fiber-Based White-Light Interferometric Sensor for High-Temperature Measurements. *Opt. Lett.* **2005**, *30*, 711–713.

(26) Grobnic, D.; Mihailov, S. J.; Smelser, C. W.; Ding, H. Sapphire Fiber Bragg Grating Sensor Made Using Femtosecond Laser Radiation for Ultrahigh Temperature Applications. *IEEE Photon. Technol. Lett.* **2004**, *16*, 2505–2507.

(27) Habisreuther, T.; Elsmann, T.; Pan, Z.; Graf, A.; Willsch, R.; Schmidt, M. A. Sapphire Fiber Bragg Gratings for High Temperature and Dynamic Temperature Diagnostics. *Appl. Therm. Eng.* **2015**, *91*, 860–865.

(28) Yang, S.; Hu, D.; Wang, A. Point-by-Point Fabrication and Characterization of Sapphire Fiber Bragg Gratings. *Opt. Lett.* **2017**, *42*, 4219–4222.

(29) Xu, X.; He, J.; Liao, C.; Yang, K.; Guo, K.; Li, C.; Zhang, Y.; Ouyang, Z.; Wang, Y. Sapphire Fiber Bragg Gratings Inscribed with a Femtosecond Laser Line-by-Line Scanning Technique. *Opt. Lett.* **2018**, *43*, 4562–4565.

(30) Xu, X.; He, J.; He, J.; Xu, B.; Chen, R.; Wang, Y.; Yang, Y.; Wang, Y. Efficient Point-by-Point Bragg Grating Inscription in Sapphire Fiber Using Femtosecond Laser Filaments. *Opt. Lett.* **2021**, *46*, 2742–2745.

(31) Xu, X.; He, J.; Liao, C.; Wang, Y. Multi-Layer, Offset-Coupled Sapphire Fiber Bragg Gratings for High-Temperature Measurements. *Opt. Lett.* **2019**, *44*, 4211–4214.

(32) Liu, B.; Yu, Z.; Hill, C.; Cheng, Y.; Homa, D.; Pickrell, G.; Wang, A. Sapphire-Fiber-Based Distributed High-Temperature Sensing System. *Opt. Lett.* **2016**, *41*, 4405–4408.

(33) Yang, S.; Homa, D.; Heyl, H.; Theis, L.; Beach, J.; Dudding, B.; Acord, G.; Taylor, D.; Pickrell, G.; Wang, A. Application of Sapphire-Fiber-Bragg-Grating-Based Multi-Point Temperature Sensor in Boilers at a Commercial Power Plant. *Sensors* **2019**, *19*, 3211.

(34) Chen, H.; Buric, M.; Ohodnicki, P. R.; Nakano, J.; Liu, B.; Chorpeneing, B. T. Review and Perspective: Sapphire Optical Fiber Cladding Development for Harsh Environment Sensing. *Appl. Phys. Rev.* **2018**, *5*, 11102.

(35) Shen, Y. H.; Tong, L. M.; Chen, S. Y. Study on Performance Stability of the Sapphire Fiber and Cladding under High Temperature. *Proceedings of SPIE*, 1999; Vol. 3852, pp 134–142.

(36) Petrie, C. M.; Blue, T. E. In Situ Thermally Induced Attenuation in Sapphire Optical Fibers Heated to 1400 °C. *J. Am. Ceram. Soc.* **2015**, *98*, 483–489.

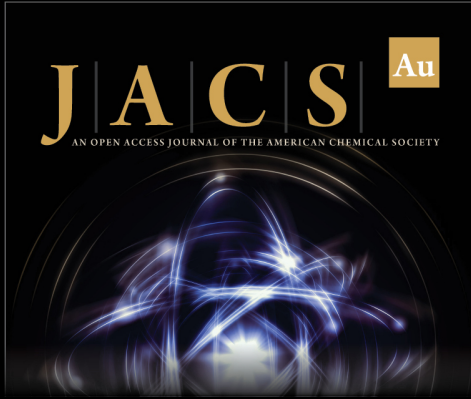
(37) Wilson, B. A.; Petrie, C. M.; Blue, T. E. High-Temperature Effects on the Light Transmission Through Sapphire Optical Fiber. *J. Am. Ceram. Soc.* **2018**, *101*, 3452–3459.

(38) Palmour, H.; Duplessis, J. J.; Kriegel, W. W. Microstructural Features and Dislocations on Thermally Etched Sapphire Surfaces. *J. Am. Ceram. Soc.* **1961**, *44*, 400–404.

(39) Fritsch, M.; Klemm, H.; Herrmann, M.; Schenk, B. Corrosion of Selected Ceramic Materials in Hot Gas Environment. *J. Eur. Ceram. Soc.* **2006**, *26*, 3557–3565.

(40) Opila, E. J.; Myers, D. L. Alumina Volatility in Water Vapor at Elevated Temperatures. *J. Am. Ceram. Soc.* **2004**, *87*, 1701–1705.

(41) Beresna, M.; Gecevičius, M.; Kazansky, P. G. Ultrafast Laser Direct Writing and Nanostructuring in Transparent Materials. *Adv. Opt. Photon.* **2014**, *6*, 293–339.



JACS Au
AN OPEN ACCESS JOURNAL OF THE AMERICAN CHEMICAL SOCIETY

Editor-in-Chief
Prof. Christopher W. Jones
Georgia Institute of Technology, USA

Open for Submissions 

pubs.acs.org/jacsau  ACS Publications
Most Trusted. Most Cited. Most Read.